Electrochemical Reduction and Oxidation of Ruddlesden–Popper-Type $La_2NiO_3F_2$ within Fluoride-Ion Batteries

Kerstin Wissel, Roland Schoch, Tobias Vogel, Manuel Donzelli, Galina Matveeva, Ute Kolb, Matthias Bauer, Peter R. Slater, and Oliver Clemens*

ABSTRACT: Within this article, it is shown that an electrochemical defluorination and additional fluorination of Ruddlesden–Popper type $La_2NiO_3F_2$ is possible within all solid state fluoride ion batteries. Structural changes within the reduced and oxidized phases have been examined by X ray diffraction studies at different states of charging and discharging. The synthesis of the oxidized phase $La_2NiO_3F_{2+x}$ proved to be successful by structural analysis using both X ray powder diffraction and automated electron diffraction tomography techniques. The structural reversibility on re fluorinating and re defluorinating is also demonstrated. Moreover, the influence of different sequences of consecutive reduction and oxidation steps on the formed phases has been investigated. The observed structural changes have been compared to changes in phases obtained via other topochemical modification approaches such as hydride based reduction and oxidative fluorination using F_2 gas, highlighting the potential of such electrochemical reactions as alternative synthesis routes. Furthermore, the electrochemical routes represent safe and controllable synthesis approaches for novel phases, which cannot be synthesized via other topochemical methods. Additionally, side reactions, occurring alongside the desired electrochemical reactions, have been addressed and the cycling performance has been studied.

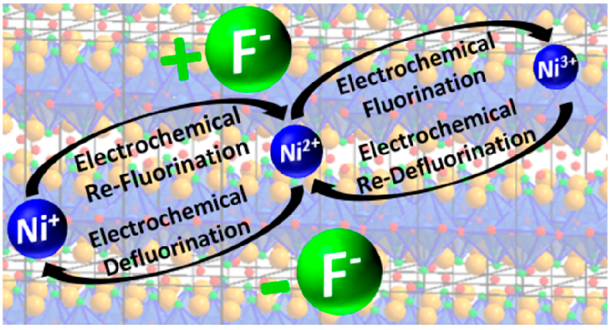

1. INTRODUCTION

Topochemical reactions to modify transition metal oxidation states of perovskite and perovskite related compounds have been extensively studied. Such reactions can be highly oxidizing by using oxidative reagents such as O_2, O_3, F_2, AgF_2, and CuF_2.[1−5] The removal of oxide or fluoride ions is possible via hydride based reductions and can lead to compounds with high contents of cations in unusual low oxidation states, such as Ni^+ or Ti^{3+}.[6−13]

Apart from chemical routes, electrochemical reactions in alkaline aqueous electrolytes have already been examined for the oxidative oxygen intercalation, which can be considered as the electrochemical equivalent to the aforementioned reactions using O_2 or O_3.[14−17] In principle, topochemical reductions can also be imagined via such electrochemical methods; however, due to the narrow stability window of aqueous electrolytes on the reductive side, an early onset of the decomposition of water with the formation of H_2 is observed. This makes a considerable reductive oxygen deintercalation impossible. Therefore, the synthesis of compounds, which can be synthesized via hydride based reductions, has not been achieved using electrochemical approaches yet.

Our group has recently shown that topochemical fluorination of Ruddlesden–Popper type (RP type) oxides can be performed within all solid state fluoride ion batteries (FIBs).[18−20] The electrolyte used $La_{0.9}Ba_{0.1}F_{2.9}$ has a broad electrochemical window,[21] which allows for oxidative fluorination. Moreover, it should also be suitable for the reductive defluorination process, since very low potentials of ~0.7 and 0.1 V against metallic lithium[22] are required for the reduction of La^{3+} and Ba^{2+}, respectively.

RP type compounds $A_{n+1}B_nO_{3n+1}\square_2$ can be described as being built up of alternate stackings of n ABO_3 perovskite layers and one AO rock salt layer.[23−25] While the equatorial and apical anion sites of the perovskite building blocks are fully occupied in stoichiometric oxides, interstitial vacancies □ are present within the rock salt layers. These interstitial vacancies can be filled by additional anions (e.g., with oxide ions in over stoichiometric oxides or with fluoride ions for the synthesis of oxyfluorides). Depending on the topochemical fluorination method used, oxidative (using, e.g., fluorine gas or electrochemical fluorination approaches) and non oxidative (using, e.g., fluorine containing polymers such as polyvinylidene difluoride

(PVDF)) fluorination reactions can be achieved.[2−4,26] The oxidative fluorination occurs via the intercalation of fluoride ions into the interstitial site, resulting in $A_{n+1}B_nO_{3n+1}F_x\square_{2-x}$ with $x \leq 2$. The non oxidative fluorination takes place when for every substituted oxide ion two fluoride ions are intercalated, leading to the formation of $A_{n+1}B_nO_{3n+1-x}F_{2x}\square_{2-x}$ with $0 < x \leq 2$. Such coupled intercalation and substitution processes can also be slightly oxidative, as has been observed when fluorinating, for example, $La_3Ni_2O_7$ to $La_3Ni_2O_{5.5}F_{3.5}$ using CuF_2 as a fluorination agent.[27]

Applying the non oxidative fluorination method, for fluorinated $n = 1$ RP type compounds with $x = 1$, it follows that there are still vacancies at anion sites. Therefore, it might be possible to fill these vacancies oxidatively in an additional electrochemical fluorination step, resulting in compounds with oxidation states and compositions, which are not accessible by conventional chemical routes. Additionally, due to the ability of these RP type oxyfluorides to either deintercalate or intercalate fluoride ions, the compound could be used as active material within anode and cathode composites in FIBs.

In this respect, $La_2NiO_3F_2$ containing Ni^{2+} is a promising candidate as active material, since Ni can also adopt oxidation states of +I and +III, which would be formed within FIBs when reducing or oxidizing the compound upon fluoride deintercalation or intercalation, respectively. $La_2NiO_3F_2$ can be prepared from La_2NiO_{4+d} via a topochemical fluorination using PVDF as described previously.[28] The oxyfluoride shows an unusually ordered channel like half occupation of the interlayer sites by oxide ions accompanied by a high degree of tilting of the NiO_4F_2 octahedra, resulting in a strong orthorhombic distortion. Its crystal structure (space group *Cccm*) is depicted in Figure 1a.

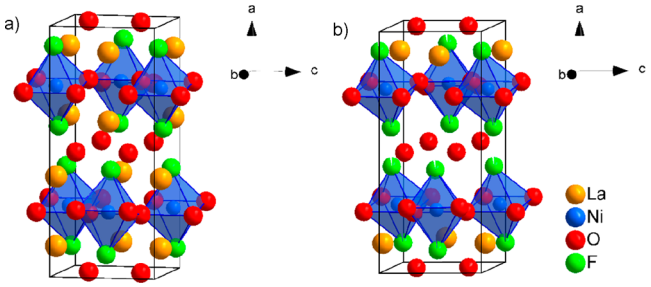

Figure 1. Crystal structure of the active material $La_2NiO_3F_2$ (a) and the monoclinic $La_2NiO_3F_{2-\Delta}$ prepared via a NaH based reduction (b).

Further, DFT based calculations predict that the redox couples $La_2NiO_3F_{2-x}|La_2NiO_3F_2$ with $0 < x \leq 1$ and $La_2NiO_3F_2|La_2NiO_3F_{2+x}$ with $0 < x \leq 1$ possess suitable potentials between ~ −0.5 and −1 V vs Pb|PbF_2 (Pb|PbF_2 possesses a potential of ~2.3 V vs Li|LiF[18]) for the extraction of fluoride[9] and between ~1.2 and 2.3 V vs Pb|PbF_2 for the intercalation of fluoride from/into $La_2NiO_3F_2$. The theoretical gravimetrical capacities of ~67 and ~64 $mAhg^{-1}$ for the extraction and intercalation of one fluoride ion, respectively, are also comparatively high.

For a structural understanding of the phases formed when reducing $La_2NiO_3F_2$ electrochemically, it is important to revisit previously reported reduced phases obtained via other topochemical reduction reactions. In a recent article,[9] our group has reported on various phases $La_2NiO_3F_{2-\Delta}H_d$ with $0 < \Delta < 1$ synthesized from $La_2NiO_3F_2$ using sodium hydride (NaH) as a reducing agent. NaH has been found to be a suitable reagent for the chemical defluorination of RP type oxyfluorides due to the low redox potential of the reductive species H^-.[7−9] The involved redox couple $2H^-|H_2$ possesses a comparatively low potential of ~0.8 V vs Li|LiF (~ −2.2 V vs $H_2|2H^+$).[22] The selective reductive extraction of fluoride ions is further promoted by the enthalpic contribution of the formed side product NaF to the change of Gibbs free energy of a respective reaction, which is also related to the difference of the lattice energies between NaH and NaF.[7] For small NaH amounts, i.e., for molar equivalents of $0 < x < 0.75$ according to the reaction equation $La_2NiO_3F_2 + xNaH$, a monoclinic phase with approximate composition $La_2NiO_3F_{1.93}$ and space group $C12/c1$ is formed (Figure 1 b). The comparatively small fluoride deficiency of $\Delta \sim 0.1$ results in significant structural changes as compared to the orthorhombic structure of the parent oxyfluoride $La_2NiO_3F_2$ due to the presence of Jahn−Teller active Ni^+, and a characteristic diffraction pattern has been observed. When using higher NaH amounts, more heavily reduced phases with higher symmetries have been additionally identified in the obtained phase mixtures. The phase fractions of these phases increase with increasing NaH amounts used. A maximum reduction to La_2NiO_3F has been found. The hydride contents within these phases, in particular for the monoclinic phase, are relatively small. Similar structural changes can be expected for electrochemically reduced RP type phases derived from $La_2NiO_3F_2$. The detailed knowledge gained about the reduction behavior and structure−property response of $La_2NiO_3F_2$ to reduction via the hydride based approach can also help to facilitate the analysis of the phases obtained after the electrochemical reduction, for which a detailed structural analysis is often unfeasible.[9]

Here, we report on the synthesis of RP type compounds $La_2NiO_3F_{2-\Delta}$ containing Ni^+ and $La_2NiO_3F_{2+\Delta}$ containing Ni^{3+} from $La_2NiO_3F_2$ via an electrochemical approach, i.e., galvanostatic charging and discharging of all solid state cells based on the solid electrolyte $La_{0.9}Ba_{0.1}F_{2.9}$. A M/MF_2 composite with M = Pb or Zn has been used as a counter electrode material. Structural changes are investigated by means of an X ray diffraction and a transmission electron microscopy study. Further, the changes are compared to those of chemically prepared equivalents, which were obtained via a hydride based reduction reported previously[9] and oxidative fluorination approaches of $La_2NiO_3F_2$ using F_2 gas, which were attempted within this study. X ray absorption spectroscopy is used to examine the Ni oxidation state of $La_2NiO_3F_{2-\Delta}$. In addition, the importance of sequences of electrochemical treatments, i.e., only charging as compared to charging and discharging to obtain the same product, are investigated and cycling performances are discussed. Moreover, side reactions seem to impede the desired defluorination and fluorination reactions of the RP type oxyfluoride. In order to investigate their nature, experiments addressing possible reactions involving $La_{0.9}Ba_{0.1}F_{2.9}$ and/or carbon black were performed. By means of X ray photoelectron spectroscopic studies and cyclic voltammetry, insights into the side reactions were gained.

Formally, during the electrochemical reduction of $La_2NiO_3F_2$, the following reaction (eq 1) should take place. Equation 2 describes the potential oxidation reaction occurring at the Pb/PbF_2 counter electrode.

$$La_2NiO_3F_2 + \Delta e^- \rightleftharpoons La_2NiO_3F_{2-\Delta} + \Delta F^- \quad (1)$$

$$Pb + 2F^- \rightleftharpoons PbF_2 + 2e^- \quad (2)$$

The electrochemical oxidation of $La_2NiO_3F_2$ and the respective reduction of Pb/PbF_2 should proceed via eqs 3 and 4.

$$La_2NiO_3F_2 + \Delta F^- \rightleftharpoons La_2NiO_3F_{2+\Delta} + \Delta e^- \quad (3)$$

$$PbF_2 + 2e^- \rightleftharpoons Pb + 2F^- \quad (4)$$

2. EXPERIMENTAL SECTION

2.1. Electrolyte and Electrode Material Preparation. The preparation of the electrolyte and electrode composites was performed using ball milling (planetary ball mill PM 100CM, Retsch). The respective educts were weighed and filled into a ZrO_2 grinding jar with ZrO_2 balls in an Ar filled glovebox. The jar was sealed before taking it out of the glovebox in order to avoid direct contact to air.

For the electrolyte $La_{0.9}Ba_{0.1}F_{2.9}$, stoichiometric ratios of LaF_3 (99.9%, STREM Chemicals) and BaF_2 (99%, STREM Chemicals) were milled for 12 h at 600 rpm. LaF_3 and BaF_2 were dried prior to their use by heating them to 700 °C under Ar.

$La_2NiO_3F_2$ was prepared from La_2NiO_{4+d} via a topochemical fluorination using PVDF as described previously.[28] It has to be pointed out that depending on the synthesis batch of $La_2NiO_3F_2$ slightly varying compositions with small amounts of not fully fluorinated $La_2NiO_{3+d/2}F_{2-d}$ can be obtained, which are then also present in the electrode mixtures. In accordance with previous reports, $La_2NiO_{3+d/2}F_{2-d}$ is formed when the parent oxide La_2NiO_{4+d} is fluorinated with slightly under stoichiometric fluorine amounts. For the preparation of the electrode composite, 30 wt % of $La_2NiO_3F_2$ was milled with 60 wt % of $La_{0.9}Ba_{0.1}F_{2.9}$ and 10 wt % of dried carbon black (CB) (99.9+%, abcr) for 1 h at 250 rpm. The electrode material containing $La_2NiO_{4.13}$ as active material was prepared in the same fashion. A mixture of thoroughly mixed $La_{0.9}Ba_{0.1}F_{2.9}$ and carbon black was prepared beforehand by milling for 3 h at 250 rpm. This mixture was also used as an electrode composite for experiments without other active materials. The electrode material containing $La_2NiO_3F_2$ as active material was used as anode or cathode materials depending on the conducted experiment. The terminology of anode and cathode is based on the role of the active material within the composite during discharge. The anode material was always used as the reference electrode.

As counter electrode, a conversion based electrode was used consisting of a metal M (M = Pb or Zn), a metal fluoride MF_2 (M = Pb or Zn), and CB. For the synthesis of the Pb/PbF_2 composite, 45 wt % Pb (≥99%, Sigma Aldrich), 45 wt % PbF_2 (99+%, STREM chemicals), and 10 wt % dried CB were milled for 12 h at 600 RP RPM. The Zn/ZnF_2 composite was prepared using the same milling procedure using 20 wt % Zn (98%, abcr), 20 wt % ZnF_2 (99%, abcr), 50 wt % $La_{9.9}Ba_{0.1}F_{2.9}$, and 10 wt % CB. $La_{9.9}Ba_{0.1}F_{2.9}$ was used to increase the ionic conductivity within the composite.

2.2. Cell Preparation and Electrochemical Defluorination and Fluorination. For the cell preparation, pellets consisting of the anode composite, electrolyte, and cathode composite were pressed using a hand held hydraulic press (Specac) with 2 t for 90 s in an Ar filled glovebox. A 5 mg portion of the electrode composite was used. Within this composite, 1.5 mg of the active material $La_2NiO_3F_2$ (or $La_2NiO_{4.13}$) and 3.5 mg of $La_{0.9}Ba_{0.1}F_{2.9}$ and carbon black, which ensure sufficient ionic and electronic conductivity, are contained. For experiments on the $La_{0.9}Ba_{0.1}F_{2.9}$ and carbon black only, i.e., where no active material was present, 3.5 mg of the $La_{0.9}Ba_{0.1}F_{2.9}$ and carbon black mixture was used. An 8 mg portion of the M/MF_2 composite corresponding to an excess was used. Specific capacities were calculated in relation to the amount of the RP type phase active material used in the electrode composite.

To ease the discussion, the cells will be referred to by the name of their respective active material in relation to the active material in the counter electrode (i.e., Pb/PbF_2 vs $La_2NiO_3F_2$ ($La_2NiO_3F_2$ is the active material in the anode composite), $La_2NiO_3F_2$ vs Pb/PbF_2 ($La_2NiO_3F_2$ is the active material in the cathode composite), Pb/PbF_2 vs $La_2NiO_{4.13}$ ($La_2NiO_{4.13}$ is the active material in the anode composite), and $La_2NiO_{4.13}$ vs Pb/PbF_2 ($La_2NiO_{4.13}$ is the active material in the cathode composite)). Cells without $La_2NiO_3F_2$ or $La_2NiO_{4.13}$ are labeled as Pb/PbF_2 vs $La_{0.9}Ba_{0.1}F_{2.9}$ + CB or $La_{0.9}Ba_{0.1}F_{2.9}$ + CB vs Pb/PbF_2. The redox couples in the electrode composites containing $La_2NiO_3F_2$ are $La_2NiO_3F_{2-x}|La_2NiO_3F_2$ (when used as the active anode material) and $La_2NiO_3F_2|La_2NiO_3F_{2+x}$ (when used as the active cathode material).

The pellets were spring loaded into modified Swagelok type cells with stainless steel current collectors (Figure 2a). A cross sectional SEM image of a typical pellet is shown in Figure 2b. The cells were heated to 170 °C to achieve sufficient ionic conductivity of the electrolyte.

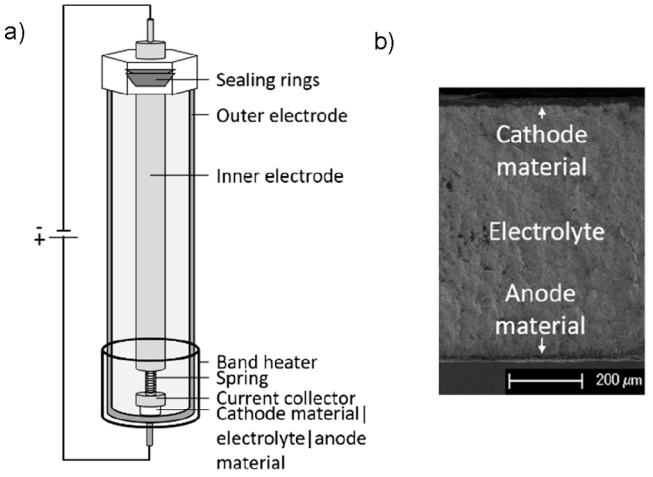

Figure 2. (a) Schematic setup of a cell; (b) cross sectional SEM image of a pellet cell Pb/PbF_2 against $La_2NiO_3F_2$.

Electrochemical experiments were performed with a VSP or SP 150 potentiostat (BioLogic Science Instruments). For galvanostatic charging and discharging, constant currents of ±2.5 mAg^{-1}(~C/25 rate) were applied. For cell cycling, cells were cycled between suitable cutoff capacities or voltages.

Cyclic voltammetry was carried out at a scan rate of 0.01 mV s^{-1} between 3 and 0 V starting from the OCV.

2.3. Fluorination Using F_2 Gas. Additional fluorination of $La_2NiO_3F_2$ was performed using flowing F_2 (10% in N_2) at temperatures between 150 and 250 °C for durations between 15 and 60 min. The schematic for the fluorine gas furnace setup can be found in ref 2. After each heat treatment, the furnace was immediately purged with N_2.

2.4. X-ray Diffraction and Rietveld Analysis. X ray diffraction data were recorded on a Bruker D8 Advance in Bragg−Brentano geometry with Cu Kα radiation and a VANTEC detector. Powder samples of $La_2NiO_{4.13}$ and $La_2NiO_3F_2$ were measured over the whole 2θ range from 5 to 130°. Air sensitive pellet samples were measured in low background airtight sample holders in a 2θ range between 20 and 70° (for $2\theta < 20°$, high background results from the sample holder; for $2\theta > 80°$, strain broadening becomes too high to resolve further reflections). For selected samples, high quality measurements (duration of 66 h) were performed additionally. Chemically defluorinated $La_2NiO_3F_{2-\Delta}H_d$ and fluorinated $La_2NiO_3F_{2+\Delta}$ were measured in airtight sample holders in the range from 20 to 130°.

Analysis of the diffraction data was performed using the Rietveld method with the program TOPAS V5.0.[29,30] The instrumental intensity distribution of the XRD instrument was determined empirically from a sort of fundamental parameter set using a reference scan of LaB_6 (NIST 660a, see Figure S23 in the Supporting Information). Rietveld refinements were performed on the full ranges measured for the respective samples (for better representation, only certain angular ranges are shown in the main article; refinements over the whole range are given in the Supporting Information). Microstructural parameters (e.g., crystallite size and strain broadening) were refined to adjust the peak shapes. Thermal displacement parameters were constrained to be the same for all atoms of all phases to minimize quantification errors and correlation with occupancy parameters.

Several reduced and oxidized RP type phases, derived from the precursor oxyfluoride $La_2NiO_3F_2$, could be identified and will be

discussed in the following manuscript. To provide the reader with an aid to follow the discussion more easily, a qualitative overview over the fluoride contents of the phases is given in Figure 3. However, we also

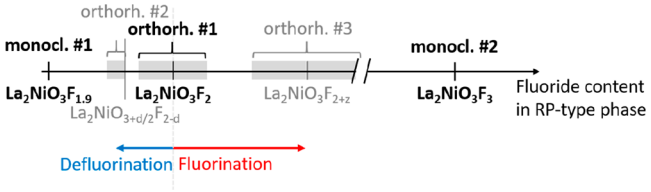

Figure 3. Schematic overview over approximate fluoride ion contents of the identified RP type phases. The detailed compositions of some phases are not known and/or are subjected to additional changes in dependence of the charging and discharging state; this is indicated by the use of ranges (gray).

would like to emphasize that a strong focus will be set on the strongest reduced phase called "monoclinic #1" and the strongest oxidized phase called "monoclinic #2".

For the Rietveld refinements, known structural models obtained via the in depth structural analyses of phase pure samples or of samples containing a high phase fraction of the respective phase, for which a variety of complementary characterization techniques have been applied, were used for the RP type phases. For the refinement of the phase called "orthorhombic #1" (i.e., the precursor oxyfluoride $La_2NiO_3F_2$), the structural model of the precursor oxyfluoride $La_2NiO_3F_2$ with the space group *Cccm*, proposed in ref 28, was used. The model for the orthorhombic #2 phase was deduced from the phase $La_2NiO_{3+d/2}F_{2-d}$ with *Fmmm* symmetry, proposed by Hancock.[31] For the phase called "orthorhombic #3", the same model as that for the orthorhombic #1 phase was used. The lattice parameters of this oxidized phase were determined based on a sample containing a high phase fraction of the phase. The model obtained from the structural analysis of chemically defluorinated $La_2NiO_3F_{1.93}$[8] was used to model the intensity profile of the electrochemically reduced monoclinic phase (called "monoclinic #1"). Both phases are isotypic. For the additionally fluorinated phase called "monoclinic #2", a model with space group *C*12/*c*1 was used for the analysis of powder diffraction data. This symmetry can be deduced via *translationengleiche and klassengleiche* symmetry reductions from the aristotype symmetry *I*4/*mmm* of RP type phases. Though one cannot be sure that this symmetry describes the correct tilting pattern of octahedra due to the fact that corresponding superstructure reflections could not be resolved in the composite mixture, it serves to confirm the correct crystal system from the splitting of the main reflections and therefore allows for the determination of lattice parameters and phase quantification. For the latter, this is explained by the fact that the weight fraction determined from the scaling parameter is less sensitive to the details of the anion sublattice and only requires good approximation of the integral intensities, which are dominated by the nearly ideal positions of the La and Ni ions. This insensitivity toward minor changes within the anion sublattice, related to the comparatively low scattering factors of oxide and fluoride ions, is also valid for the other phases considered in this work. Using these structural models, stable refinements could be obtained. The structural parameters of the used models can be found in the respective references and in addition Tables S1, 2, 3, 5, and 9 in the Supporting Information.

2.5. X-ray Absorption Spectroscopy. X ray absorption spectroscopy (XAS) experiments at the Ni K edge (8333 eV) were carried out at the DESY (Deutsches Elektronen Synchrotron) beamline P64 in Hamburg, Germany. The measurements were performed using a Si(111) double crystal monochromator and a maximum synchrotron beam current of 100 mA. Due to the low Ni concentration, all spectra were recorded in fluorescence mode. Additionally, a Co filter (3 μm thickness) was applied to reduce interference radiation on the detector. For energy calibration, a Ni foil was measured in advance and after the sample spectra to account for possible energy shifts due to monochromator movements. The energy shift was detected at the edge energies, which were determined by the maxima in the spectrum derivations, as well as in the energies of the prepeaks.

To achieve a sufficient amount of $La_2NiO_3F_{2-\Delta}$ for XANES measurements, 8 cells Pb/PbF_2 vs $La_2NiO_3F_2$ were charged to 75 $mAhg^{-1}$ and the electrode sides containing $La_2NiO_3F_{2-\Delta}$ were scratched off the pellets. The obtained powder was subsequently mixed with dried boron nitride at the beamline facility and pressed to pellets. The complete handling of the samples (preparation and measurement) was carried out under an inert atmosphere to minimize re oxidation of the electrode material.

2.6. X-ray Photoelectron Spectroscopy. The surface oxidation states were examined by X ray photoelectron spectroscopy (XPS) analysis on a Physical Electronic VersaProbe XPS unit (PHI 5000 spectrometer) with Al Kα radiation (1486.6 eV). To confirm the calibration of the instrument, gold (Au $4f_{7/2}$ emission line at 84.0 eV) and silver (Ag $3d_{5/2}$ emission line at 368.3 eV) were measured as reference materials beforehand. All detailed spectra were recorded with a step size of 0.1 eV and a pass energy of 23.5 eV at an electron escape angle of 75° and a spot size of 200 × 200 μm^2. A neutralizer was used for the compensation of surface charge effects by using low energy electrons and Ar ions.

The binding energy of the C 1s emission line of the pristine anode composite was found to be at ~284.4 eV, which is a typical binding energy of carbon black.[32] Due to expected shifts of the carbon signals of the reduced and oxidized samples, the C 1s line could not be used to calibrate the samples. Since shifts in the F 1s signal should be small, the F 1s emission line was used for the calibration of the reduced and oxidized samples. When doing so, the La and Ni lines, which are dominated by the La signal from the stable (and, therefore, unaffected by chemical shifts) electrolyte $La_{0.9}Ba_{0.1}F_{2.9}$, also aligned. Due to the strong signal of La, a deconvolution of the La and Ni signals was not possible. The found binding energies of the La $3d_{5/2}$, La $3d_{3/2}$, and F 1s signals agree well with reference values of the signals of LaF_3, which is close to that of the dominating phase $La_{0.9}Ba_{0.1}F_{2.9}$.[33−36] The Ni 3p lines could not be used for the determination of the oxidation state due to their very low intensities.

Samples were transferred from an Ar filled glovebox to the ultrahigh vacuum system of the spectrometer in Ar atmosphere using a sealed transfer chamber capable of in vacuo transportation to minimize surface oxidation processes.

3. RESULTS AND DISCUSSION

3.1. Electrochemical Reduction of $La_2NiO_3F_2$. A typical charging curve of the Pb/PbF_2 composite against the $La_2NiO_3F_2$ composite is shown in Figure 4. The Pb/PbF_2 composite was

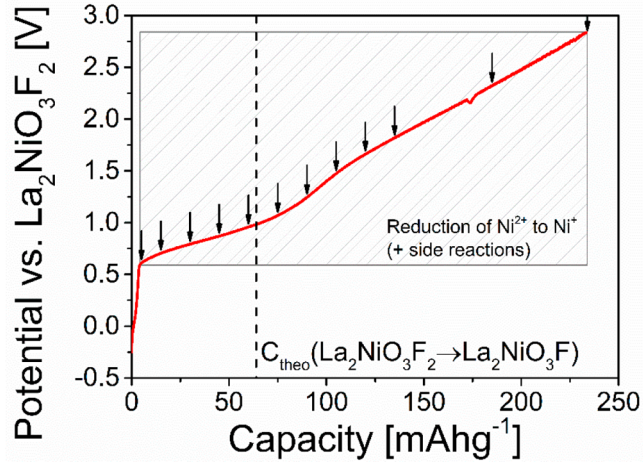

Figure 4. Charging curve of a cell Pb/PbF_2 against $La_2NiO_3F_2$. The arrows show various cutoff capacities, to which different cells were charged.

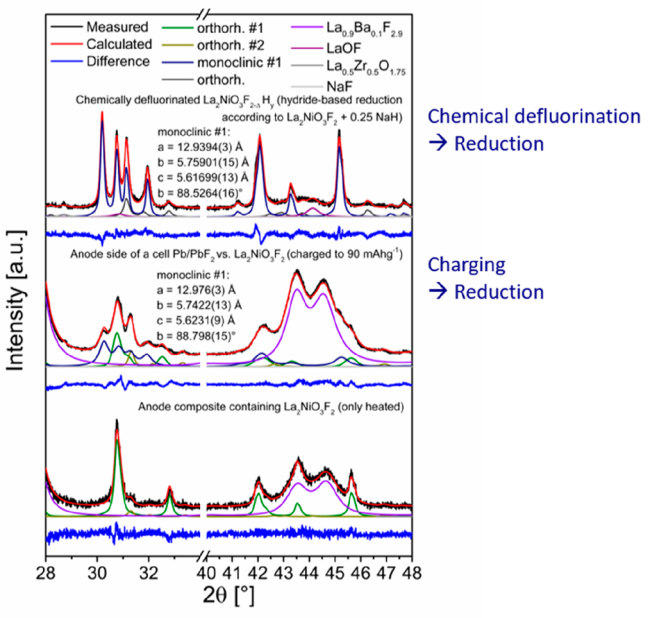

Figure 5. Selected angular ranges of Rietveld refinements of the anode composite containing $La_2NiO_3F_2$ (only heated) (bottom), an electro chemically reduced anode side of a cell Pb/PbF_2 against $La_2NiO_3F_2$ (charged to 90 $mAhg^{-1}$) (middle), and chemically reduced $La_2NiO_3F_{2-\Delta}H_y$ (hydride based defluorination according to the reaction equation $La_2NiO_3F_2 + xNaH$, with $x = 0.25$) (top). For full refinements and lattice parameters, phase fraction, etc., see Supporting Information Figure S2b and l, Figure S3, and Table S4.

used as cathode material and the $La_2NiO_3F_2$ composite as anode material. Since the theoretical capacity for the extraction of one fluoride ion from $La_2NiO_3F_2$ is ~67 $mAhg^{-1}$, it is clearly indicated that besides the desired reduction of $La_2NiO_3F_2$ other redox processes in the form of undesired side reactions occur (see section 3.4).

In order to obtain insight into the structural changes of $La_2NiO_3F_2$ at different charging states, several cells have been charged to different cutoff capacities (Figure 4) and X ray diffraction patterns (see Supporting Information Figure S1 for an overview of all diffraction patterns) were collected ex situ and analyzed using the Rietveld method (see Supporting Information Figure S2 for all Rietveld refinements, Table S4 for lattice parameters, phase fractions, etc., and Figure S4 for the evolution of lattice parameters).

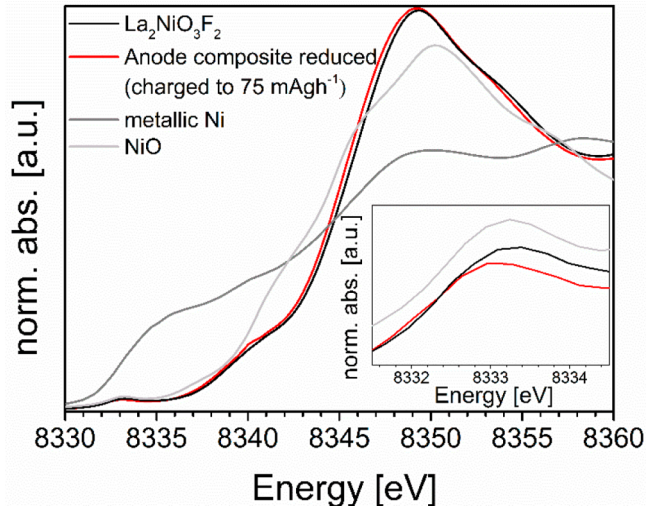

Figure 7. X ray absorption spectra of $La_2NiO_3F_2$ and $La_2NiO_3F_{2-\Delta}$. As a reference, the spectra of Ni foil and NiO are plotted.

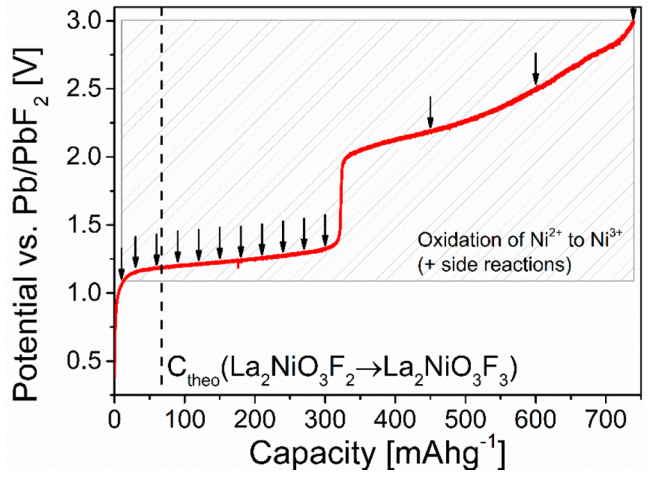

Figure 8. Charging curve of a cell $La_2NiO_3F_2$ against Pb/PbF_2. The arrows show various cutoff capacities to which different cells were charged.

The RP type phases in the electrode composite are stable upon heating, highlighting the need to apply currents to induce compositional and/or structural changes. After charging,

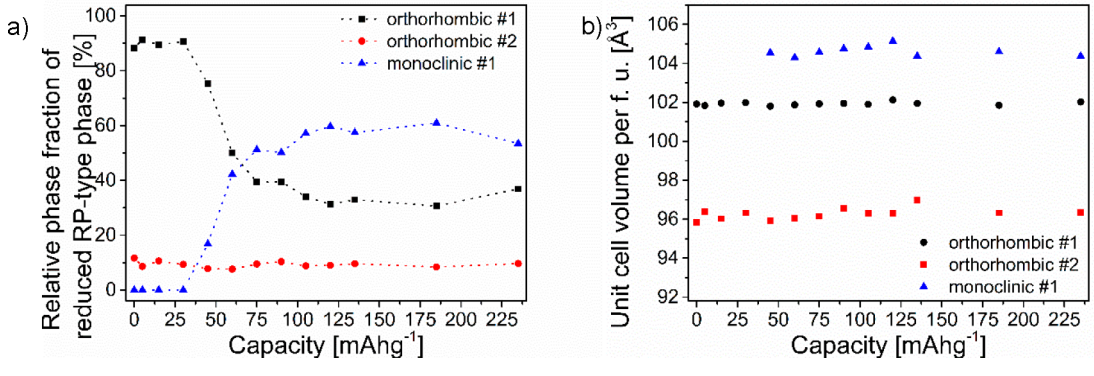

Figure 6. Relative phase fractions (a) and unit cell volume per formula unit (b) of reduced RP type orthorhombic #1, orthorhombic #2, and monoclinic #1 phases in the anode sides of cells Pb/PbF_2 against $La_2NiO_3F_2$ charged to different cutoff capacities. For the calculation of the relative phase fractions of the RP type phases to one another, the phase fraction of $La_{0.9}Ba_{0.1}F_{2.9}$ has not been taken into account.

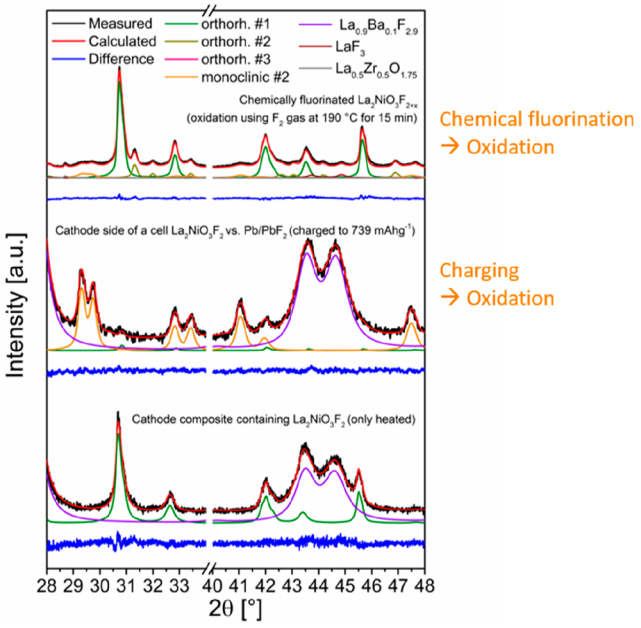

Figure 9. Selected angular ranges of Rietveld refinements of the cathode composite containing $La_2NiO_3F_2$ (only heated) (bottom), an electrochemically reduced cathode side of a cell $La_2NiO_3F_2$ against Pb/PbF_2 (charged to 739 $mAhg^{-1}$) (middle), and chemically oxidized $La_2NiO_3F_{2+x}$ (F_2 gas oxidation according to the reaction equation $La_2NiO_3F_2 + x/2\ F_2$) (top). For full refinements and lattice parameters, phase fraction, etc., see Supporting Information Figure S7a and o, Figure S11, and Table S6).

substantial changes have been observed (Figure 5). With increasing degree of reductive defluorination ($C > 30$ $mAhg^{-1}$), a monoclinic phase (called "monoclinic #1") occurs, which will be shown to be structurally identical to monoclinic $La_2NiO_3F_{1.93}$, obtained via a hydride based reduction, in the next paragraph. Its phase fraction increases strongly until ~75 $mAhg^{-1}$, while the phase fraction of the main starting phase $La_2NiO_3F_2$ (called "orthorhombic #1") decreases and remains constant at higher charging states thereafter (Figure 6a). The cell volumes per formula unit (f. u.) of the individual RP type phases remain relatively constant over the whole capacity range (Figure 6b). The highest unit cell volume is observed for the monoclinic #1 phase. On formation of this phase from the orthorhombic #1 phase, a steep increase in cell volume of ~3 $Å^3$ per formula unit is found. This increase is due to expansions along the *a* axis and within the *bc* plane. The latter mainly affects the equatorial Ni−O bonds, in consistency with the previously reported detailed structural analysis of this compound prepared via a NaH based chemical defluorination.[9]

The comparison between the X ray diffraction patterns of the charged (to 90 $mAhg^{-1}$) anode composite and chemically defluorinated $La_2NiO_3F_{1.93}$[9] (Figure 5) shows that the electro chemically formed monoclinic #1 phase is in excellent agreement with what is found when reducing $La_2NiO_3F_2$ via the hydride based reaction. No indication is given for the formation of stronger defluorinated, orthorhombic phases, found when reducing $La_2NiO_3F_2$ chemically, even when charging to the highest capacities.

To confirm the change of the oxidation state of the reduced RP type phases, XANES spectra of pure $La_2NiO_3F_2$ and of the electrochemically reduced anode composite (charged to 75 $mAhg^{-1}$) (Figure 7) have been measured and compared. For the reduced cells, a small energy shift of the adsorption edge of ~0.5 eV to lower binding energies is observed and confirms that a partial reduction of $La_2NiO_3F_2$ to $La_2NiO_3F_{2-\Delta}$ has occurred. The shift is in the right order of magnification with respect to what would be expected for the formation of ~10% Ni^+ within the reduced phase, reflecting a change of the oxidation state from +2 to ~ +1.9. For comparison, it has been reported that the reduction of the structurally related n = 2 and 3 RP type nickelates $La_3Ni_2O_{6.9}$ and $La_4Ni_3O_{10}$ result in shifts of ~2−3 eV upon the chemical deoxygenation to $La_3Ni_2O_6$ and $La_4Ni_3O_8$, correlated to the reduction of the Ni oxidation state from +2.4 to +1.5 and +2.67 to +1.33, respectively.[10,11]

From the analysis of diffraction data in combination with the reduction indicated by XAS, it can be concluded that the electrochemically obtained phase has indeed a composition of approximately $La_2NiO_3F_{1.9}$.

Complementary XPS measurements (see Supporting Information Figure S5) give no meaningful information about the oxidation state of Ni of the electrochemically reduced RP type phases due to the small energy separation between the La 3d and Ni 2p (or La 4d and Ni 3s signals).[37,38]

3.2. Electrochemical Oxidation of $La_2NiO_3F_2$. The charging curve of a cell, in which the $La_2NiO_3F_2$ composite is charged against the Pb/PbF_2 composite ($La_2NiO_3F_2$ is used as active cathode material), is shown in Figure 8. Two distinctive plateaus can be distinguished. As for the electrochemical reduction of $La_2NiO_3F_2$, the observed capacities strongly exceed

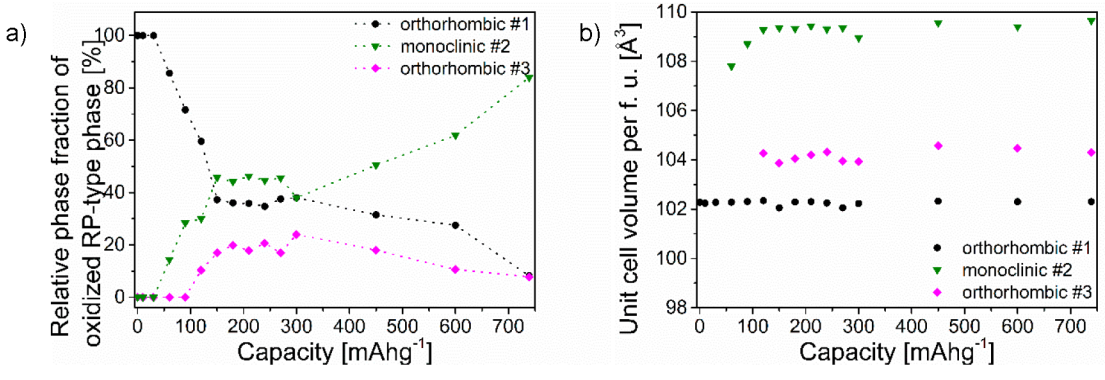

Figure 10. Relative phase fractions (a) and unit cell volume per formula unit (b) of oxidized RP type orthorhombic #1, monoclinic #2, and orthorhombic # 3 phases in the cathode sides of cells Pb/PbF_2 against $La_2NiO_3F_2$ charged to different cutoff capacities. For the calculation of the relative phase fractions of the RP type phases to one another, the phase fraction of $La_{0.9}Ba_{0.1}F_{2.9}$ has not been taken into account.

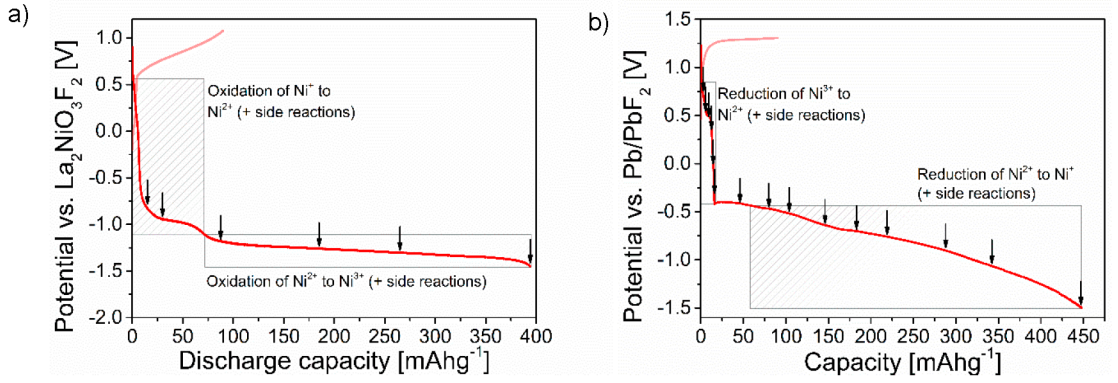

Figure 11. Charging and discharging curves of a cell Pb/PbF_2 against $La_2NiO_3F_2$ (a) and of a cell $La_2NiO_3F_2$ against Pb/PbF_2 (b). Both cells were charged to 90 $mAhg^{-1}$ and subsequently discharged. The arrows show various cutoff capacities to which different cells were discharged. The shaded regions indicate where oxidation and reduction reactions of the RP type phases (+ side reactions) take place and which Ni species are involved.

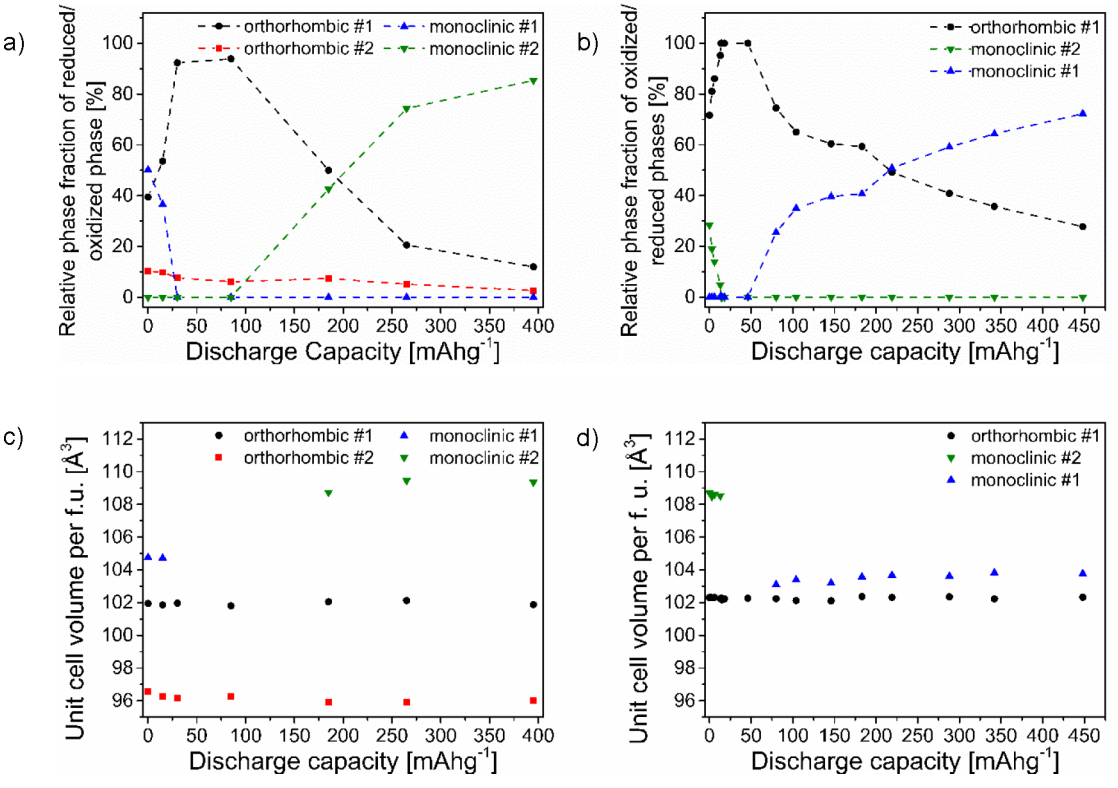

Figure 12. Relative phase fractions and unit cell volume per formula unit of reduced/oxidized RP type orthorhombic #1, orthorhombic #2, monoclinic #1, and monoclinic #2 phases in anode sides of cells Pb/PbF_2 against $La_2NiO_3F_2$ (a and c) and on cathode sides of cells $La_2NiO_3F_2$ against Pb/PbF_2 (b and d). Both cells were charged to 90 $mAhg^{-1}$ and subsequently discharged to different cutoff capacities. For the calculation of the relative phase fractions of the RP type phases to one another, the phase fraction of $La_{0.9}Ba_{0.1}F_{2.9}$ has not been taken into account.

the theoretical capacity for the intercalation of one additional fluoride ion of ~64 $mAhg^{-1}$. Therefore, undesired side reactions have to take place, as has also been previously reported for the electrochemical fluorination of intercalation based RP type cathodes.[18,19,39]

In the same fashion as for the defluorination of $La_2NiO_3F_2$, X ray diffraction patterns of cathode sides of cells charged to different cutoff capacities (Figure 8), containing differently strong oxidized phases, have been measured and analyzed (see Supporting Information Figure S6 for an overview of all diffraction patterns, Table S6 for lattice parameters, phase fractions, etc., and Figure S8 for the evolution of lattice parameters). The Rietveld refinements of all measurements are given in Figure S7 in the Supporting Information.

Electrochemical fluorination upon charging leads for $C > 30$ $mAhg^{-1}$ to the appearance of a monoclinic phase (called "monoclinic #2", Figure 9) and an orthorhombic phase (called "orthorhombic #3") (Figure 9a). Along with these observations, a continuous decrease of the phase fraction of the orthorhombic #1 phase up to ~150 $mAhg^{-1}$ takes place. Only for much higher capacities ($C \gg 300$ $mAhg^{-1}$, corresponding to the second plateau in the charging curve), further changes of the phase fractions are observed, resulting in an additional formation of the monoclinic #2 phase at the cost of the orthorhombic #1 and #3 phases. Since the monoclinic #2 phase is partly formed from the

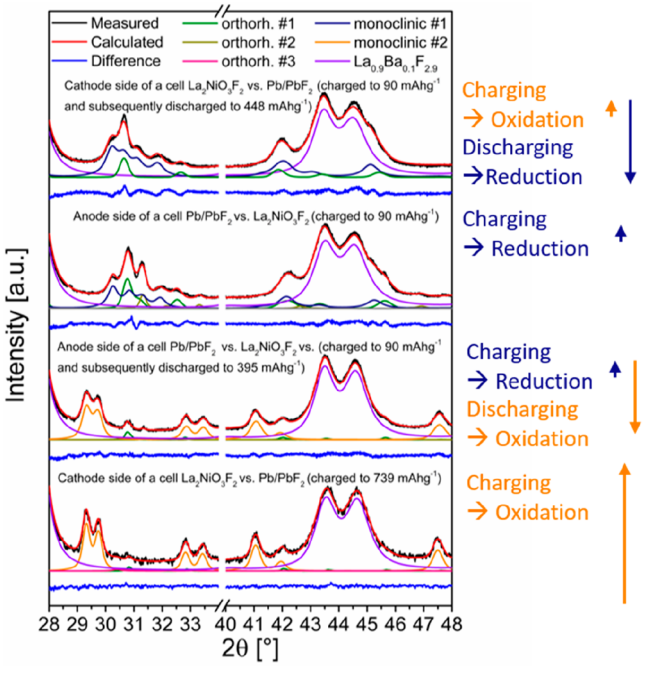

Figure 13. Selected angular ranges of Rietveld refinements of an electrochemically oxidized cathode side of a cell $La_2NiO_3F_2$ against Pb/PbF_2 (charged to 739 $mAhg^{-1}$) (bottom), an electrochemically reduced and subsequently oxidized anode side of a cell Pb/PbF_2 against $La_2NiO_3F_2$ (charged to 90 $mAhg^{-1}$ and subsequently discharged to 395 $mAhg^{-1}$) (second from bottom), an electrochemically reduced anode side of a cell Pb/PbF_2 against $La_2NiO_3F_2$ (charged to 90 $mAhg^{-1}$) (second from top), and an electrochemically oxidized and subsequently reduced cathode side of a cell $La_2NiO_3F_2$ against Pb/PbF_2 (charged to 90 $mAhg^{-1}$ and subsequently discharged to 448 $mAhg^{-1}$) (top). For full refinements and lattice parameters, phase fraction, etc., see Supporting Information Figures S2i, S3, S7o, and S15f and Tables S4, S6, S10, and S11).

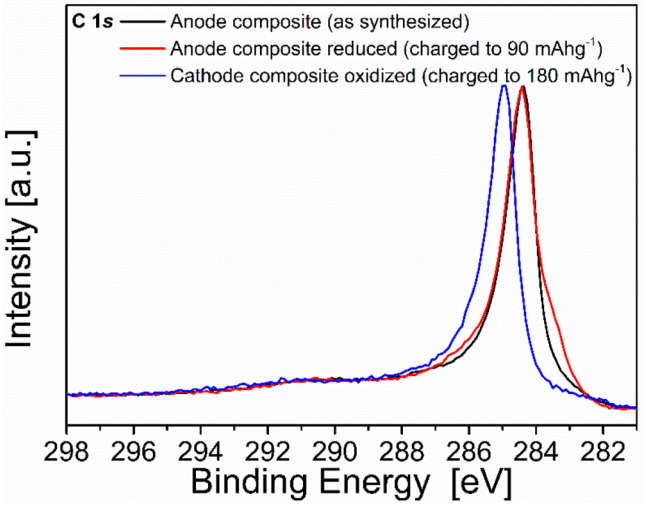

Figure 14. Normalized C 1s XPS spectra of the anode composite (as synthesized), the anode side of a cell Pb/PbF_2 against $La_2NiO_3F_2$ (charged 90 $mAhg^{-1}$), and the cathode side of a cell $La_2NiO_3F_2$ against Pb/PbF_2 (charged 180 $mAhg^{-1}$).

orthorhombic #3 phase at higher capacities, it can be followed that the monoclinic #2 phase has a higher fluoride content than the orthorhombic #3 phase. The cell volumes of each phase are again relatively independent of the state of charging (Figure 10b), with the exception for the lower charging states ($C < 150$ $mAhg^{-1}$) of the monoclinic #2 phase. For this phase, a continuous increase of the lattice parameter a and, consequently, of the cell volume is found for capacities up to ~150 $mAhg^{-1}$. A volume increase of up to ~7 $Å^3$ per formula unit as compared to the orthorhombic #1 phase is found. This increase of a indicates that a strong change of the anion sublattice occurs, which is most likely due to an increased filling of the vacant interstitial site, present in $La_2NiO_3F_2$, by fluoride, leading to the formation of $La_2NiO_3F_3$. A filling of the interstitial site could also be confirmed using transmission electron diffraction (the structural model used for the refinements is given in Supporting Information Table S9; see also Supporting Information Figures S12 and S13 and Tables S7 and S8). Such expansions along the long crystallographic axis have been commonly observed, when the interstitial sites of RP type compounds have been filled by additional anions.[40−42] In addition, a contraction of the bc plane suggests strong changes of bond distances of equatorial Ni−O bonds, which would be expected for an oxidation to Ni^{3+}, which is smaller than Ni^{2+}.[43] Based on these structural changes and the observed symmetry, a composition close to $La_2NiO_3F_3$ is considered most plausible for the monoclinic #2 phase.

In analogy to the reduction of $La_2NiO_3F_2$, a comparison between chemically and electrochemically prepared equivalents of the oxidized phases is interesting (Figure 9). It becomes, however, evident that the chemical fluorination of $La_2NiO_3F_2$ using highly oxidizing F_2 gas results only in a very small fraction of $La_2NiO_3F_{2+x}$, while the predominant phase (~90 wt %) is still unreacted $La_2NiO_3F_2$. Longer exposure to F_2 or higher reaction temperatures causes a complete decomposition of $La_2NiO_3F_2$, leading to the formation of LaF_3, whereas lower reaction temperatures at increased reaction time do not lead to any changes of the parent phase (see Supporting Information Figures S9 and S10). The found oxidized phase is in good agreement with the electrochemically formed monoclinic #2 phase. The electrochemical fluorination results, however, in considerably higher phase fractions of the fluorinated monoclinic phase. Therefore, electrochemical routes can present viable, safe, and easily controllable methods for the synthesis of fluorinated compounds, which cannot be obtained via other routes.

3.3. Electrochemical Re-Oxidation/Re-Reduction of Reduced/Oxidized RP-Type Phases. Re oxidation of the reduced RP type phases has been performed in Pb/PbF_2 against $La_2NiO_3F_2$ cells, which were previously charged to 90 $mAhg^{-1}$. Due to strong overpotentials, a considerable discharging can only be obtained when the cells are discharged to negative potentials (Figure 11a). Within the first observed discharging plateau between ~ −0.8 and −1.1 V against $La_2NiO_3F_2$, the orthorhombic #1 and #2 starting phases are regained and the monoclinic #1 phase vanishes completely (Figure 12a, and see Supporting Information Figure S14 for an overview of all diffraction patterns, Figure S15 for the Rietveld refinements of all measurements, Table S10 for lattice parameters, phase fractions, etc., and Figure S16 for the evolution of lattice parameters). This confirms the reversibility of the structural changes on re fluorination. Considering that the charging of the cell to 90 $mAhg^{-1}$ results in the formation of a relative phase fraction of only ~50% of the partially reduced Ni^+ containing monoclinic #1 phase, the first charging plateau related to the re oxidation of the Ni^+ species is too long, suggesting that side reactions take place as well. Forcing the cells to discharge beyond this first discharging plateau, a second extended plateau

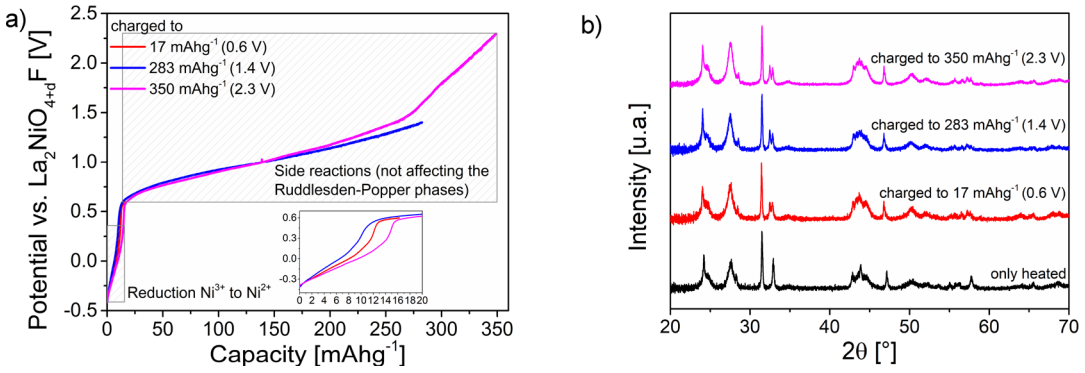

Figure 15. (a) Charging curves of cells Pb/PbF_2 against $La_2NiO_{4.13}$ obtained at a rate of C/25. The cells were charged to 17, 283, and 350 $mAhg^{-1}$, respectively. (b) X ray diffraction patterns of the anode sides of different Pb/PbF_2 against $La_2NiO_{4.13}$ charged to 17, 283, and 350 $mAhg^{-1}$. For reference, a cell that has been only heated is given. The refinements and lattice parameters, phase fraction, etc., are given in Supporting Information Figure S13 and Table S12).

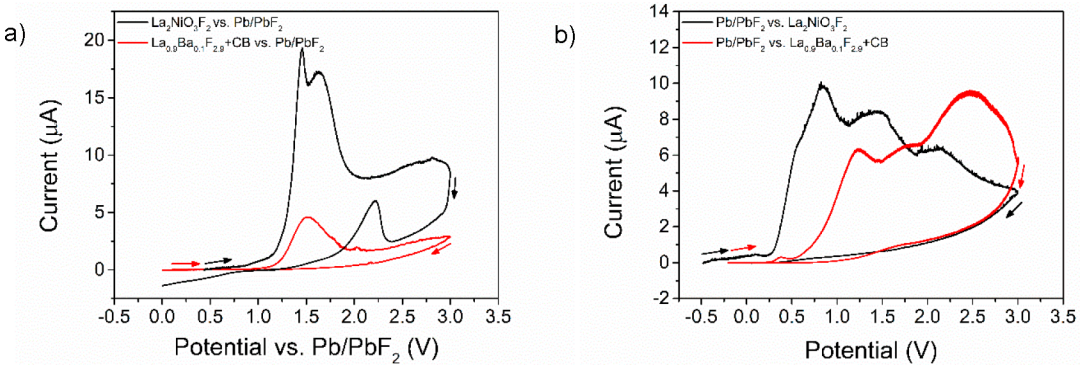

Figure 16. Cyclic voltammograms of cells $La_2NiO_3F_2$ vs Pb/PbF_2 and $La_{0.9}Ba_{0.1}F_{2.9}$ + CB vs Pb/PbF_2 (a) and cells Pb/PbF_2 vs $La_2NiO_3F_2$ and Pb/PbF_2 vs $La_{0.9}Ba_{0.1}F_{2.9}$ + CB (b).

occurs. In the diffraction pattern of the extendedly discharged cell (Figure 13), strong changes resulting from the formation of the monoclinic #2 phase are observed. The same phase has been observed for a direct fluorination of the respective cathode composite. The phase fraction of the monoclinic #2 phase increases continuously, while the other phases diminish (Figure 12a). For all phases, the unit cell volumes (Figure 12c) are in good agreement with what has been found in sections 3.1 and 3.2.

Similar to the re oxidation of the reduced RP type phases, re reduction experiments on the oxidized phases have been performed via discharging of previously defluorinated (charged to 90 $mAhg^{-1}$) $La_2NiO_3F_2$ against Pb/PbF_2 cells. In this case, a first discharging plateau is located within the positive potential range between ~0.55 and 0.45 V against Pb/PbF_2 (Figure 11b). Within this plateau, the orthorhombic #1 starting phase is fully regained and the monoclinic #2 phase disappears (Figure 12b, and see Supporting Information Figure S17 for an overview of all diffraction patterns, Figure S18 for the Rietveld refinements of all measurements, Table S11 for lattice parameters, phase fractions, etc., and Figure S19 for the evolution of lattice parameters). This shows that a full structural reversibility is found for charging and discharging within the positive potential range, making the cathode composite a promising candidate for its application in reversible intercalation based FIBs (see section 3.5). With respect to the relative phase fraction of the monoclinic #2 phase of ~30% found within the cathode side of the cell after charging and its composition close to $La_2NiO_3F_3$, the corresponding theoretical discharge capacity for the reduction of Ni^{3+} to Ni^{2+} is in good agreement with the observed length of the first discharging plateau. Side reactions seem to play a minor role. Further discharging to negative potentials leads to the occurrence of a second extended sloping plateau between ~ −0.35 and −1.5 V. The formation of the monoclinic #1 phase can be followed from the changes of the X ray diffraction pattern (Figure 13). The same phase has also been observed after the direct defluorination of the anode composite (see section 3.1). The cell volumes are given in Figure 12d.

When comparing the relative phase fractions of the observed RP type phases and the capacities needed to obtain these phases, interesting trends can be found with respect to different sequences of electrochemical treatments. The reduction of $La_2NiO_3F_2$ followed by its oxidation leads to considerably higher phase fractions of the monoclinic #2 phase at much lower capacities and potentials compared to the direct oxidation of the cathode material (Figure 13). The results suggest that a partial defluorination facilitates the electrochemical fluorination process of $La_2NiO_3F_2$, leading to the increased formation of $La_2NiO_3F_{2+x}$ with Ni^{3+}. This might result from anion disorder introduced on the defluorination of the starting material aiding anion migration and thus facilitating the formation of the highly fluorinated state. A similar effect has been observed for a sequence of an oxidation step followed by a reduction step (Figure 13). However, even though larger phase fractions of the monoclinic #1 phase are obtained after discharging to 448 $mAhg^{-1}$, the influence of the previous oxidation of $La_2NiO_3F_2$ on the formation of the reduced monoclinic #1 phase seems to

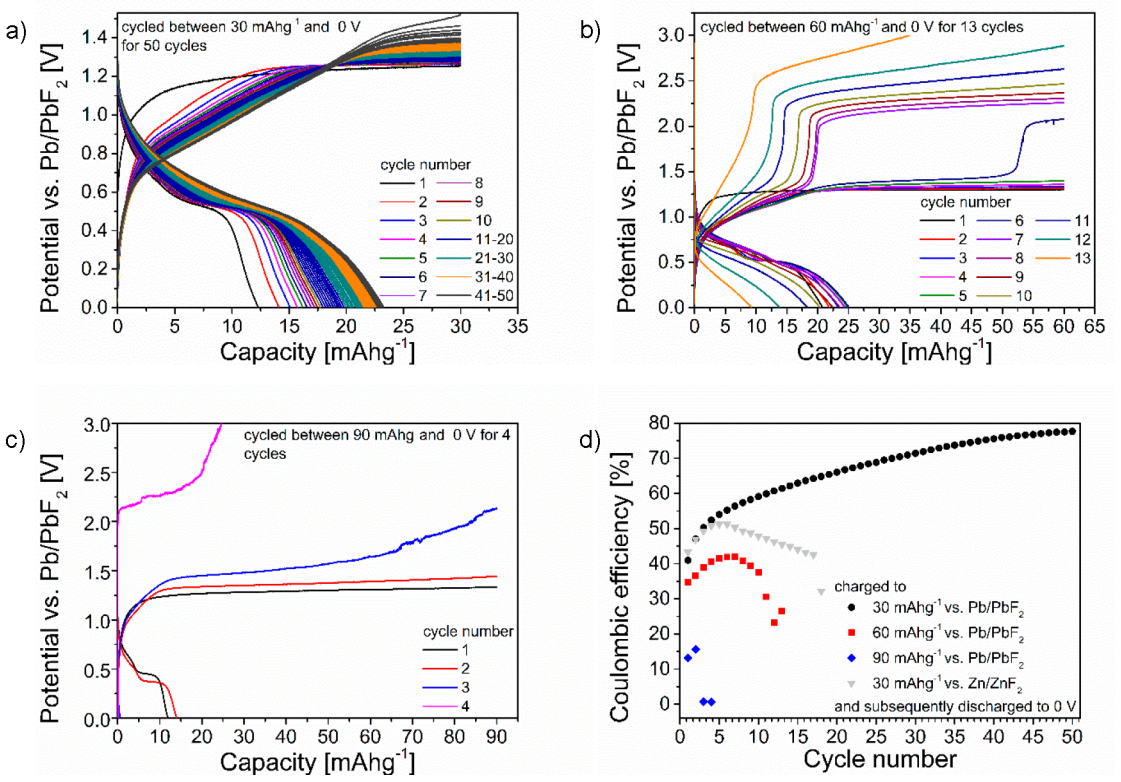

Figure 17. (a–c) Cycling curves of cells $La_2NiO_3F_2$ against Pb/PbF_2 obtained at a rate of C/25. The cells were cycled between different cutoff capacities of 30 $mAhg^{-1}$ (a), 60 $mAhg^{-1}$ (b), and 90 $mAhg^{-1}$ (c) and the cutoff voltage of 0 V. (d) Coulombic efficiencies of cells $La_2NiO_3F_2$ against Pb/PbF_2 cycled between different cutoff charging capacities of 30, 60, and 90 $mAhg^{-1}$ and the discharging cutoff voltage of 0 V. Additionally, the Coulombic efficiencies of a cell $La_2NiO_3F_2$ against Zn/ZnF_2 cycled between the cutoff charging capacities of 30 $mAhg^{-1}$ and the cutoff discharging voltage of 0 V is given.

not be as severe as for the opposite sequence of reduction and oxidation. The much higher discharge capacity of 448 $mAhg^{-1}$ as compared to the charge capacity of only 90 $mAhg^{-1}$ of the directly reduced cell has to be taken into account. This limited influence might be related to the smaller extent of introduced disorder in the fluorinated material due to the intercalation of additional fluoride ions into interstitial vacancies.

3.4. Investigation of Side Reactions. When comparing theoretical capacities for the extraction and intercalation of one fluoride ion to the obtained capacities of the reduction and oxidation experiments, it is apparent that side reactions are taking place, which do not affect the RP type phases.

Grenier et al.[21] observed an electrochemical activity of the carbon within a composite with the electrolyte at potentials between ~4.2 and 4.8 V vs Li (~1.9–2.5 V vs Pb/PbF_2), which leads to an irreversible fluorination of C, related to the formation of electronic insulating CF_x species. This shows that the electrochemical window needs to be narrowed to avoid the carbon fluorination. Recently, it has been shown that in electrode composites, containing in addition an RP type active material, the carbon fluorination sets in at lower potentials, suggesting a catalytic effect of the RP type phase on the fluorination behavior of carbon.[39] The same observation has been made for cells $La_2NiO_3F_2$ vs Pb/PbF_2 in the current study. In agreement with the previous report by Nowroozi et al.,[39] a characteristic shift of the C 1s carbon signal toward higher binding energies by ~0.5 eV has been found after the oxidation of the cathode composite, indicating also the occurrence of the carbon fluorination (Figure 14). The pristine electrode composite possesses a C 1s signal at ~284.4 eV, which is characteristic for carbon black.[32] Interestingly, the spectrum of the reduced anode composite features also a shoulder at lower binding energies. This suggests that also a partial reduction of the carbon takes place during the charging of the anode material. A possible reduction of the carbon additive could take place due to a release of surface adsorbed oxygen or via a reaction with La or Ba of the electrolyte and could also cause side reactions alongside the actual reduction of the active material.

The existence of side reactions on related materials, which cannot be defluorinated, can further be evidenced on investigating the reduction of $La_2NiO_{4.13}$ within Pb/PbF_2 against $La_2NiO_{4.13}$ cells (Figure 15, see Supporting Information Figure S20 and Table S12). Here, only the reduction to orthorhombic La_2NiO_4 (space group *Bmab*),[44] i.e., the reduction from Ni^{3+} to Ni^{2+}, is observed between ~ −0.3 and 0.3 V vs $La_2NiO_{4.13}$, showing that interstitial oxide can also be deintercalated using the FIB setup. No additional structural changes of the RP type phase (Figure 15b) occur when charging beyond a subsequent plateau (~0.6–1.5 V vs $La_2NiO_{4.13}$). This plateau is, therefore, purely related to side reactions. It also coincides with the plateau observed for the electrochemical reduction of $La_2NiO_3F_2$, which indicates that alongside the actual reduction of $La_2NiO_3F_2$ side reactions take place, which do not affect the RP type phases further.

In order to differentiate in which potential range the fluorination of the active material and/or the carbon additive occurs, cyclic voltammograms of cells with electrode composites with or without the active material were recorded (Figure 16). It can be followed that a clear separation between the oxidation (Figure 16a) and reduction (Figure 16b) of the active material

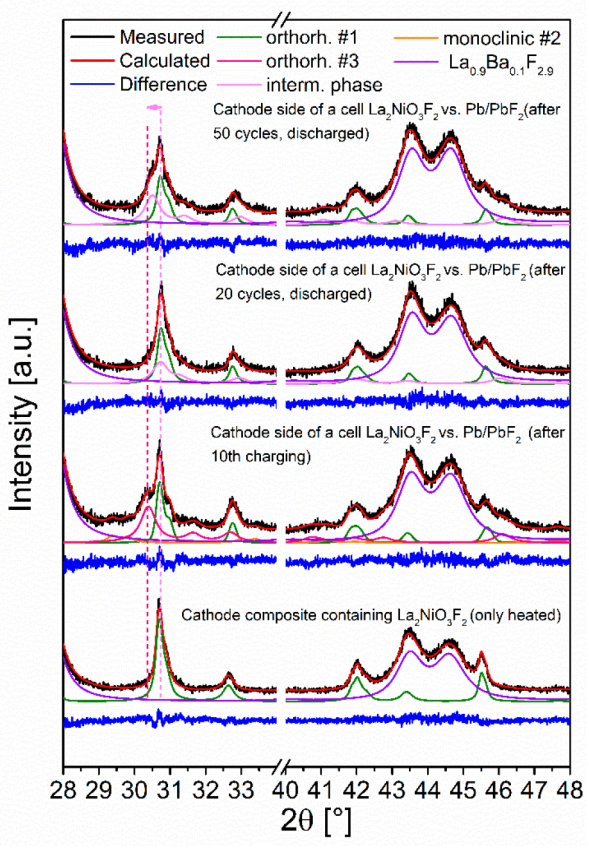

Figure 18. Selected angular ranges of Rietveld refinements of the cathode composite containing $La_2NiO_3F_2$ (only heated) (bottom), a cycled cathode side of a cell $La_2NiO_3F_2$ against Pb/PbF_2 (after 9 cycles and 10th discharging) (2nd from bottom), a cycled cathode side of a cell $La_2NiO_3F_2$ against Pb/PbF_2 (after 20 cycles) (3rd from bottom), and a cycled cathode side of a cell $La_2NiO_3F_2$ against Pb/PbF_2 (after 50 cycles) (top). For full refinements and lattice parameters, phase fraction, etc., see Supporting Information Figure S15 and Table S13). The cells were cycled between the cutoff charging capacity of 30 $mAhg^{-1}$ and the cutoff discharging voltage of 0 V.

and the side reaction involving the carbon additive is not possible. In the cell $La_{0.9}Ba_{0.1}F_{2.9}$ + CB vs Pb/PbF_2, the fluorination of carbon seems to be irreversible, since no current is observed in the anodic branch, whereas a certain reversibility is found for the $La_2NiO_3F_2$ vs Pb/PbF_2 cell. This suggests that the carbon fluorination is also irreversible in cells containing the active material. Cyclic voltammograms of cells Pb/PbF_2 against $La_2NiO_3F_2$ and Pb/PbF_2 vs $La_{0.9}Ba_{0.1}F_{2.9}$ + CB (Figure 16b) confirm the findings obtained for the reduction of $La_2NiO_{4.13}$. The reduction of the CB in the cell Pb/PbF_2 vs $La_{0.9}Ba_{0.1}F_{2.9}$ + CB seems to be widely overlapping with the electrochemical activity recorded for the cell Pb/PbF_2 against $La_2NiO_3F_2$ containing $La_2NiO_3F_2$ and CB. For both cells, no reversibility is observed.

3.5. Cell Cycling. Cell cycling was performed on cells $La_2NiO_3F_2$ against Pb/PbF_2, for which a structural reversibility of the starting phase is found when discharging within the positive potential range (see section 3.3). Cells have been charged to cutoff capacities of 30, 60, and 90 $mAhg^{-1}$ and subsequently discharged to 0 V. Cycling curves are given in Figure 17a–c. The choice of suitable cutoff charging capacities plays herein an important role. The best charging behavior is found for low charging capacities of 30 $mAhg^{-1}$, while the cells with higher charging capacities fail significantly faster. An early onset of the second plateau at low capacities is observed for the cycled cells charged to higher capacities. This indicates either that considerable amounts of the cathode composite containing the electrochemically active $La_2NiO_3F_2$ have peeled off possibly due to larger volume changes related to higher charging states or that the occurring side reactions hinder the reversible intercalation and deintercalation of fluoride ions in consecutive cycles with increasing cycle numbers. In this respect, the progressive formation of insulating CF_x species,[39] which takes place simultaneously with the fluorination of the RP type phase and becomes more dominant at higher capacities, impedes the long term cycling performance. For cells only charged to the cutoff capacity of 30 $mAhg^{-1}$, the side reactions seem to be less pronounced, leading to a longer cyclability with up to 50 cycles. This is further confirmed by the Coulombic efficiencies (Figure 17d), which give information about the extent of irreversible side reactions. Even though the efficiencies are relatively low for the cells charged to 30 $mAhg^{-1}$, the cells charged to 60 and 90 $mAhg^{-1}$ possess significantly lower efficiencies. Interestingly, the Coulombic efficiencies increase for all cells for increasing cycle numbers before they fail. Especially for the cell charged to 30 $mAhg^{-1}$, a significant increase of the efficiency of ~36% over the first 50 cycles can be observed. This increase may be related to an activation of additional storage sites, from which eventually more fluoride ions can be extracted.

It has been shown that the use of Zn/ZnF_2 as a counter electrode can improve the cycling performance of intercalation based RP type cathode materials, e.g., La_2CoO_4 or $La_2NiO_{4.13}$.[39,45] When, however, charging $La_2NiO_3F_2$ against Zn/ZnF_2 instead of Pb/PbF_2, considerably worse cycling performances are obtained with increasing overpotentials and significant capacity fading after the fifth cycle (for more details, see Supporting Information Figure S21).

To investigate structural changes of cells cycled between 30 $mAhg^{-1}$ and 0 V with respect to the cycle number, cells were cycled for various cycles and stopped either in their charged or in their discharged states. In accordance with section 3.2, after the first charging to 30 $mAhg^{-1}$, no significant structural changes are observed (see Supporting Information Figure S22 and Table S13). For higher cycle numbers, cells in the charged state show considerable amounts of the fluorinated monoclinic #2 and orthorhombic #3 phases. This might indicate that substantial fluorination is only obtained after a few cycles, in agreement with the low Coulombic efficiencies within the first cycles. Interestingly, for higher cycle numbers (Figure 18), the repeated reversible intercalation seems to result primarily in the reversible formation of the orthorhombic #3 phase. This is in contrast to the only charged cells (see section 3.2), for which the monoclinic #2 phase is dominating.

For cycled cells in the discharged state, the orthorhombic #1 starting phase is regained and the fluorinated monoclinic #2 and orthorhombic #3 phases disappear. Moreover, after cycling over 20 and 50 cycles (Figure 18), an additional intermediate phase is found besides the orthorhombic #1 phase in the discharged state of the cell. This phase exhibits a considerably lower unit cell volume than the fluorinated phases, indicating that it contains a smaller amount of fluoride ions. However, a complete defluorination to form the orthorhombic #1 phase upon discharging seems to be impossible after highly extended cycling. The phase fraction and the unit cell volume of the intermediate phase is additionally found to increase between the 20th and the 50th cycle significantly.

4. CONCLUSIONS

In summary, the new compounds $La_2NiO_3F_{2-\Delta}$ containing Ni^+ and $La_2NiO_3F_{2+\Delta}$ containing Ni^{3+} can be synthesized using galvanostatic charging and discharging within all solid state FIBs. This highlights the potential of electrochemical routes as alternative methods for the topochemical modification of perovskite and perovskite related compounds, which are very difficult to obtain using chemical routes. This is facilitated by the high stability of the solid electrolyte $La_{0.9}Ba_{0.1}F_{2.9}$ toward reduction and oxidation. In contrast to hydride based reactions, electrochemical defluorination reactions result in the formation of materials free of hydride species. In addition, electrochemical fluorination of $La_2NiO_3F_2$ is the only feasible route for the preparation of $La_2NiO_3F_3$.

Structural reversibility on re fluorination and re defluorination has also been demonstrated. Moreover, continued discharging to potentials lower than the potentials needed for the re fluorination and re defluorination leads to the formation of the respective additionally fluorinated or defluorinated compound from the re fluorinated or re defluorinated compounds. Especially for the re fluorination of pre reduced $La_2NiO_3F_2$, the continued fluorination leads to the formation of high phase fractions of $La_2NiO_3F_{2+\Delta}$, which cannot be obtained via the direct fluorination of $La_2NiO_3F_2$. This highlights the influence of the chosen electrochemical sequence with a potential role of the introduction of anion disorder on the resulting products. Furthermore, combined approaches of electrochemical defluorination and fluorination do represent a new viable method to prepare novel materials, which cannot be easily prepared using classical chemical routes.

Side reactions of the carbon additive have been shown to occur alongside the defluorination and fluorination reactions and seem to compete with the desired reactions. This is also reflected in the cycling performance of $La_2NiO_3F_2$ vs Pb/PbF_2 cells. Reversible battery operation could be demonstrated over up to 50 cycles.

■ ASSOCIATED CONTENT

X ray diffraction patterns of anode sides of different cells Pb/PbF_2 vs $La_2NiO_3F_2$ charged to various cutoff capacities; structural parameters of the orthorhombic #1, orthorhombic #2, and monoclinic #1 phases; Rietveld refinements of precursor oxyfluoride contained in anode composite $La_2NiO_3F_2$ and of electrochemically reduced anode sides of cells Pb/PbF_2 vs $La_2NiO_3F_2$; Rietveld refinement of chemically reduced $La_2NiO_3F_{2-\Delta}H_y$; quantitative analysis and refined lattice parameters and unit cell volumes of $La_2NiO_3F_2$, chemically reduced $La_2NiO_3F_{2-\Delta}H_y$ (hydride based reduction), anode composite containing $La_2NiO_3F_2$ (only heated), and anode sides of different cells Pb/PbF_2 vs $La_2NiO_3F_2$ charged to different cutoff capacities; lattice parameters *a*, *b*, and *c* of reduced RP type phases in the anode sides of cells Pb/PbF_2 against $La_2NiO_3F_2$ charged to different cutoff capacities; normalized F 1s, La 3d (Ni 2p), La 4d (Ni 3s), Ni 3p, and O 1s X ray photoelectron spectra of the anode composite containing $La_2NiO_3F_2$ (as synthesized), of an anode side of a cell Pb/PbF_2 vs $La_2NiO_3F_2$ charged to 90 mAh^{-1}, and of a cathode side of a cell $La_2NiO_3F_2$ vs Pb/PbF_2 charged to 180 $mAhg^{-1}$; X ray diffraction patterns of cathode sides of different cells $La_2NiO_3F_2$ against Pb/PbF_2 charged to various cutoff capacities; structural parameters of the orthorhombic #3 phase; Rietveld refinement of electrochemically oxidized cathode sides of cells $La_2NiO_3F_2$ vs Pb/PbF_2; X ray diffraction patterns of chemically oxidized $La_2NiO_3F_{2+x}$ obtained after exposure of $La_2NiO_3F_2$ to F_2 gas at different reaction temperatures for a duration of 15 min; quantitative analysis and refined lattice parameters and unit cell volumes of chemically oxidized $La_2NiO_3F_2$ (F_2 gas fluorination) and cathode composite containing $La_2NiO_3F_2$ (only heated) and cathode sides of different cells $La_2NiO_3F_2$ vs Pb/PbF_2 charged to different cutoff capacities; lattice parameters *a*, *b*, and *c* of oxidized RP type orthorhombic #1, monoclinic #2, and orthorhombic # 3 phases in the cathode sides of cells Pb/PbF_2 against $La_2NiO_3F_2$ charged to different cutoff capacities; X ray diffraction patterns of chemically oxidized $La_2NiO_3F_{2+x}$ obtained after exposure of $La_2NiO_3F_2$ to F_2 gas at a reaction temperature of 190 °C for different durations; Rietveld refinement of chemically oxidized $La_2NiO_3F_{2+\Delta}$ obtained after exposure of $La_2NiO_3F_2$ to F_2 gas at a reaction temperature of 190 °C for a duration of 15 min; EDX spectrum of the measured crystal in μ STEM NED mode confirming the presence of Ni within the crystal; views of the reciprocal space along the directions from left to right (100), (010), (001) of the monoclinic #2 phase, measured using ADT; lattice parameters derived for ADT measurements of the monoclinic #2 phase; crystallographic information about ADT measurement and structure solution of $La_2NiO_3F_3$ with SIR2014; structural parameters of the oxidized monoclinic #2 phase; X ray diffraction patterns of anode sides of different cells Pb/PbF_2 against $La_2NiO_3F_2$ charged to 90 $mAhg^{-1}$ and subsequently discharged to various cutoff capacities; Rietveld refinement of electrochemically reduced and subsequently oxidized anode sides of cells Pb/PbF_2 vs $La_2NiO_3F_2$; quantitative analysis and refined lattice parameters and unit cell volumes of anode sides of different cells Pb/PbF_2 vs $La_2NiO_3F_2$ charged to 90 $mAhg^{-1}$ and subsequently discharged to different cutoff capacities; lattice parameters *a*, *b*, and *c* of reduced/oxidized RP type orthorhombic #1, orhorhombic #2, monoclinic #1, and monoclinic #2 phases in anode sides of cells Pb/PbF_2 against $La_2NiO_3F_2$ charged to 90 $mAhg^{-1}$ and subsequently discharged to different cutoff capacities; X ray diffraction patterns of cathode sides of different cells $La_2NiO_3F_2$ against Pb/PbF_2 charged to 90 $mAhg^{-1}$ and subsequently discharged to various cutoff capacities; Rietveld refinement of electrochemically oxidized and subsequently reduced cathode sides of cells $La_2NiO_3F_2$ vs Pb/PbF_2; quantitative analysis and refined lattice parameters and unit cell volumes of cathode sides of different cells $La_2NiO_3F_2$ vs Pb/PbF_2 charged to 90 $mAhg^{-1}$ and subsequently discharged to different cutoff capacities; lattice parameters *a*, *b*, and *c* of oxidized/reduced RP type orthorhombic #1, monoclinic #2, and monoclinic #1 phases in cathode sides of cells Pb/PbF_2 against $La_2NiO_3F_2$ charged to 90 $mAhg^{-1}$ and subsequently discharged to different cutoff capacities; Rietveld refinement of the electrode composite containing $La_2NiO_{4.13}$ and of the electrochemically reduced

anode side of a cell Pb/PbF_2 vs $La_2NiO_{4.13}$; quantitative analysis and refined lattice parameters and unit cell volumes of La_2NiO_{4+d} electrode composite containing $La_2NiO_{4.13}$ and anodes of different cells Pb/PbF_2 vs $La_2NiO_{4.13}$ charged to different cutoff capacities; cycling curves and Rietveld refinement of the cathode side of a cell $La_2NiO_3F_2$ vs Zn/ZnF_2 cycled between the cutoff charging capacity of 30 $mAhg^{-1}$ and the cutoff discharging voltage of 0 V for 18 cycles; cycling curves and Rietveld refinements of the cathode side of cells $La_2NiO_3F_2$ against Pb/PbF_2 cycled between the cutoff charging capacity of 30 $mAhg^{-1}$ and the cutoff discharging voltage of 0 V for various cycles; quantitative analysis and refined lattice parameters and unit cell volumes of cathode sides of different cells $La_2NiO_3F_2$ vs Pb/PbF_2 cycled for various cycle numbers between the cutoff charging capacity of 30 $mAhg^{-1}$ and cutoff discharging voltage of 0 V; Rietveld analysis of NIST 660a LaB_6 standard (PDF)

AUTHOR INFORMATION

Corresponding Author

Oliver Clemens − *Institute for Materials Science, Materials Synthesis Group, University of Stuttgart, 70569 Stuttgart, Germany; Institute for Nanotechnology, Karlsruhe Institute of Technology, 73644 Eggenstein Leopoldshafen, Germany;* orcid.org/0000 0002 0860 0911;
Email: oliver.clemens@imw.uni stuttgart.de; Fax: +49 711 685 51933

Authors

Kerstin Wissel − *Institute for Materials Science, Materials Synthesis Group, University of Stuttgart, 70569 Stuttgart, Germany;* orcid.org/0000 0003 4418 0595

Roland Schoch − *Department Chemie, Universität Paderborn, 33098 Paderborn, Germany;* orcid.org/0000 0003 2061 7289

Tobias Vogel − *Institut für Materialwissenschaft, Fachgebiet Dünne Schichten, Technical University of Darmstadt, 64287 Darmstadt, Germany;* orcid.org/0000 0003 0720 0681

Manuel Donzelli − *Institute for Materials Science, Materials Synthesis Group, University of Stuttgart, 70569 Stuttgart, Germany*

Galina Matveeva − *Institut für Physikalische Chemie, Centre for High Resolution Electron Microscopy, Johannes Gutenberg Universität Mainz, 55128 Mainz, Germany*

Ute Kolb − *Institut für Physikalische Chemie, Centre for High Resolution Electron Microscopy, Johannes Gutenberg Universität Mainz, 55128 Mainz, Germany; Institut für Angewandte Geowissenschaften, Technical University of Darmstadt, Fachgebiet Elektronenkristallographie, 64287 Darmstadt, Germany*

Matthias Bauer − *Department Chemie, Universität Paderborn, 33098 Paderborn, Germany;* orcid.org/0000 0002 9294 6076

Peter R. Slater − *School of Chemistry, University of Birmingham, Birmingham B15 2TT, United Kingdom*

Notes

The authors declare no competing financial interest.

ACKNOWLEDGMENTS

This work was funded by the German Research Foundation within the Emmy Noether program (Grant No. CL551/2 1). K.W. acknowledges funding from the JUICED Hub researcher mobility fund (EPSRC grant EP/R023662/1).

REFERENCES

(1) Hayashi, N.; Yamamoto, T.; Kageyama, H.; Nishi, M.; Watanabe, Y.; Kawakami, T.; Matsushita, Y.; Fujimori, A.; Takano, M. $BaFeO_3$: A Ferromagnetic Iron Oxide. *Angew. Chem., Int. Ed.* **2011**, *50* (52), 12547−12550.

(2) Slater, P.; Driscoll, L. Modification of Magnetic and Electronic Properties, in Particular Superconductivity, by Low Temperature Insertion of Fluorine into Oxides. *Progr Fluor Sci. Ser.* **2016**, *1*, 401−421.

(3) Clemens, O.; Slater, P. R. Topochemical modifications of mixed metal oxide compounds by low temperature fluorination routes. *Rev. Inorg. Chem.* **2013**, *33* (2−3), 105.

(4) Greaves, C.; Francesconi, M. G. Fluorine insertion in inorganic materials. *Curr. Opin. Solid State Mater. Sci.* **1998**, *3* (2), 132−136.

(5) Greaves, C. K. J. L.; Francesconi, M. G.; Aikens, L. D.; Gillie, J. L. Synthetic strategies for new inorganic oxide fluorides and oxidesulfates. *J. Mater. Chem.* **1999**, *9*, 111−116.

(6) Hayward, M. A.; Green, M. A.; Rosseinsky, M. J.; Sloan, J. Sodium hydride as a powerful reducing agent for topotactic oxide dein tercalation: Synthesis and characterization of the nickel(I) oxide $LaNiO_2$. *J. Am. Chem. Soc.* **1999**, *121* (38), 8843−8854.

(7) Wissel, K.; Dasgupta, S.; Benes, A.; Schoch, R.; Bauer, M.; Witte, R.; Fortes, A. D.; Erdem, E.; Rohrer, J.; Clemens, O. Developing intercalation based anode materials for fluoride ion batteries: top ochemical reduction of $Sr_2TiO_3F_2$ via a hydride based defluorination process. *J. Mater. Chem. A* **2018**, *6* (44), 22013−22026.

(8) Wissel, K.; Vogel, T.; Dasgupta, S.; Fortes, A. D.; Slater, P. R.; Clemens, O. Topochemical Fluorination of n = 2 Ruddlesden Popper Type $Sr_3Ti_2O_7$ to $Sr_3Ti_2O_5F_4$ and Its Reductive Defluorination. *Inorg. Chem.* **2020**, *59* (2), 1153−1163.

(9) Wissel, K.; Malik, A. M.; Vasala, S.; Plana Ruiz, S.; Kolb, U.; Slater, P. R.; da Silva, I.; Alff, L.; Rohrer, J.; Clemens, O. Topochemical Reduction of $La_2NiO_3F_2$: The First Ni Based Ruddlesden Popper n = 1 T′ Type Structure and the Impact of Reduction on Magnetic Ordering. *Chem. Mater.* **2020**, *32* (7), 3160−3179.

(10) Poltavets, V. V.; Lokshin, K. A.; Croft, M.; Mandal, T. K.; Egami, T.; Greenblatt, M. Crystal structures of $Ln_4Ni_3O_8$ (Ln = La, Nd) triple layer T' type nickelates. *Inorg. Chem.* **2007**, *46* (25), 10887−10891.

(11) Poltavets, V. V.; Lokshin, K. A.; Dikmen, S.; Croft, M.; Egami, T.; Greenblatt, M. $La_3Ni_2O_6$: a new double T' type nickelate with infinite $Ni^{1+/2+}O_2$ layers. *J. Am. Chem. Soc.* **2006**, *128* (28), 9050−9051.

(12) Lacorre, P. Passage from T Type to T' Type Arrangement to by Reducing $R_4Ni_3O_{10}$ to $R_4Ni_3O_8$ (R = La, Pr, Nd). *J. Solid State Chem.* **1992**, *97*, 495−500.

(13) Crespin, M.; Levitz, P.; Gatinea, L. Reduced Forms of $LaNi0_3$ Perovskite Part 1. Evidence for New Phases: $La_2Ni_20_5$ and $LaNiO_2$. *J. Chem. Soc., Faraday Trans. 2* **1983**, *79*, 1181−1194.

(14) Grenier, J. C.; Pouchard, M.; Wattiaux, A. Electrochemical synthesis: oxygen intercalation. *Curr. Opin. Solid State Mater. Sci.* **1996**, *1* (2), 233−240.

(15) Demourgues, A.; Weill, F.; Grenier, J. C.; Wattiaux, A.; Pouchard, M. Electron microscopy study of electrochemically prepared $La_2NiO_{4+\delta}$ ($0.17 \leq \delta \leq 0.26$). *Phys. C* **1992**, *192* (3), 425−434.

(16) Grenier, J. C.; Wattiaux, A.; Demourgues, A.; Pouchard, M.; Hagenmuller, P. Electrochemical oxidation: a new way for preparing high oxidation states of transition metals. *Solid State Ionics* **1993**, *63−65*, 825−832.

(17) Wattiaux, A.; Fournès, L.; Demourgues, A.; Bernaben, N.; Grenier, J. C.; Pouchard, M. A novel preparation method of the $SrFeO_3$ cubic perovskite by electrochemical means. *Solid State Commun.* **1991**, *77* (7), 489−493.

(18) Nowroozi, M. A.; Wissel, K.; Rohrer, J.; Munnangi, A. R.; Clemens, O. LaSrMnO4: Reversible Electrochemical Intercalation of Fluoride Ions in the Context of Fluoride Ion Batteries. *Chem. Mater.* **2017**, *29* (8), 3441−3453.
(19) Nowroozi, M. A.; Ivlev, S.; Rohrer, J.; Clemens, O. La_2CoO_4: a new intercalation based cathode material for fluoride ion batteries with improved cycling stability. *J. Mater. Chem. A* **2018**, *6* (11), 4658−4669.
(20) Vasala, S.; Jakob, A.; Wissel, K.; Waidha, A. I.; Alff, L.; Clemens, O. Reversible Tuning of Magnetization in a Ferromagnetic Ruddlesden Popper Type Manganite by Electrochemical Fluoride Ion Intercalation. *Advanced Electronic Materials* **2020**, *6* (2), 1900974.
(21) Grenier, A.; Porras Gutierrez, A. G.; Body, M.; Legein, C.; Chrétien, F.; Raymundo Piñero, E.; Dollé, M.; Groult, H.; Dambournet, D. Solid Fluoride Electrolytes and Their Composite with Carbon: Issues and Challenges for Rechargeable Solid State Fluoride Ion Batteries. *J. Phys. Chem. C* **2017**, *121* (45), 24962−24970.
(22) Vanysek, P. Electrochemical Series. In *CRC Handbook of Chemistry and Physics*; Haynes, W. M., Ed; CRC Press: Boca Raton, FL, 2013; Chapter 5, pp 80−89.
(23) Ruddlesden, S. N.; Popper, P. New compounds of the K_2NiF_4 type. *Acta Crystallogr.* **1957**, *10* (8), 538−539.
(24) Ruddlesden, S. N.; Popper, P. The compund $Sr_3Ti_2O_7$ and its structure. *Acta Crystallogr.* **1958**, *11*, 54−55.
(25) Beznosikov, B. V.; Aleksandrov, K. S. Perovskite like crystals of the Ruddlesden Popper series. *Crystallogr. Rep.* **2000**, *45* (5), 792−798.
(26) McCabe, E. E.; Greaves, C. Review: Fluorine insertion reactions into pre formed metal oxides. *J. Fluorine Chem.* **2007**, *128*, 448−458.
(27) Zhang, R.; Senn, M. S.; Hayward, M. A., Directed Lifting of Inversion Symmetry in Ruddlesden Popper Oxide Fluorides: Toward Ferroelectric and Multiferroic Behavior. *Chem. Mater.* 2016, DOI: 10.1021/acs.chemmater.6b03931.
(28) Wissel, K.; Heldt, J.; Groszewicz, P. B.; Dasgupta, S.; Breitzke, H.; Donzelli, M.; Waidha, A. I.; Fortes, A. D.; Rohrer, J.; Slater, P. R.; Buntkowsky, G.; Clemens, O. Topochemical Fluorination of La_2NiO_{4+d}: Unprecedented Ordering of Oxide and Fluoride Ions in $La_2NiO_3F_2$. *Inorg. Chem.* **2018**, *57* (11), 6549−6560.
(29) *Diffrac.suite User Manual TOPAS 5*; Bruker AXS: Karlsruhe, Germany, 2014.
(30) Coelho, A. A. TOPAS Academic. http://www.topas academic.net (accessed October 20, 2014).
(31) Hancock, C. A. Anion substitution in Perovskite related materials for fuel cell applications. Ph.D. thesis, University of Birmingham, Birmingham, U.K., 2012.
(32) Moulder, J. F.; Chastain, J. *Handbook of X ray Photoelectron Spectroscopy: A Reference Book of Standard Spectra for Identification and Interpretation of XPS Data*; Perkin Elmer Corporation, Physical Electronics Division: Eden Prairie, MN, 1992.
(33) De Marco, R.; Cattrall, R. W.; Liesegang, J.; Nyberg, G. L.; Hamilton, I. C. XPS studies of the fluoride ion selective electrode membrane LaF_3: Ion interferences. *Surf. Interface Anal.* **1989**, *14* (8), 457−462.
(34) Shen, W.; Wang, X. D.; Cattrall, R. W.; Nyberg, G. L.; Liesegang, J. XPS analysis of hydroxide ion surface reactions on reactions on CeF_3 and LaF_3 fluoride ion selective electrodes. *Electroanalysis* **1997**, *9* (12), 917−921.
(35) Li, C.; Liu, X.; Yang, P.; Zhang, C.; Lian, H.; Lin, J. LaF_3, CeF_3, CeF_3:Tb^{3+}, and CeF_3:Tb^{3+}@LaF_3 (Core Shell) Nanoplates: Hydro thermal Synthesis and Luminescence Properties. *J. Phys. Chem. C* **2008**, *112* (8), 2904−2910.
(36) Selvasekarapandian, S.; Vijayakumar, M.; Gnanasekaran, T.; Fujihara, S.; Koji, S. Ion conduction studies on LaF_3 thin film by impedance spectroscopy. *Phys. B* **2003**, *337* (1), 52−57.
(37) Qiao, L.; Bi, X. Direct observation of Ni^{3+} and Ni^{2+} in correlated $LaNiO_{3-\delta}$ films. *EPL (Europhysics Letters)* **2011**, *93* (5), 57002.
(38) Ning, X.; Wang, Z.; Zhang, Z. Fermi level shifting, charge transfer and induced magnetic coupling at $La_{0.7}Ca_{0.3}MnO_3$/$LaNiO_3$ interface. *Sci. Rep.* **2015**, *5*, 8460.
(39) Nowroozi, M. A.; Wissel, K.; Donzelli, M.; Hosseinpourkahvaz, N.; Plana Ruiz, S.; Kolb, U.; Schoch, R.; Bauer, M.; Malik, A. M.; Rohrer, J.; Ivlev, S.; Kraus, F.; Clemens, O. High cycle life all solid state fluoride ion battery with La_2NiO_{4+d} high voltage cathode. *Communi cations Materials* **2020**, *1* (1), 27.
(40) Aikens, L. D.; Gillie, L. J.; Li, R. K.; Greaves, C. Staged fluorine insertion into manganese oxides with Ruddlesden Popper structures: $LaSrMnO_4F$ and $La_{1.2}Sr_{1.8}Mn_2O_7F$. *J. Mater. Chem.* **2002**, *12* (2), 264−267.
(41) Aikens, L. D.; Li, R. K.; Greaves, C. The synthesis and structure of a new oxide fluoride, $LaSrMnO_4F$, with staged fluorine insertion. *Chem. Commun.* **2000**, No. 21, 2129−2130.
(42) Slater, P. R.; Gover, R. K. B. Synthesis and structure of the new oxide fluoride $Sr_2TiO_3F_2$ from the low temperature fluorination of Sr_2TiO_4: an example of a staged fluorine substitution/insertion reaction. *J. Mater. Chem.* **2002**, *12* (2), 291−294.
(43) Shannon, R. D. Revised Effective Ionic Radii and Systematic Studies of Interatomie Distances in Halides and Chaleogenides. *Acta Crystallogr., Sect. A: Cryst. Phys., Diffr., Theor. Gen. Crystallogr.* **1976**, *32*, 751.
(44) Rodriguez Carvajal, J.; Fernandez Diaz, M. T.; Martinez, J. L. Neutron diffraction study on structural and magnetic properties of La_2NiO_4. *J. Phys.: Condens. Matter* **1991**, *3*, 3215−3234.
(45) Nowroozi, M. A.; Clemens, O. Insights on the Behavior of Conversion Based Anode Materials for Fluoride Ion Batteries by Testing against an Intercalation Based Reference Cathode. *ACS Applied Energy Materials* **2018**, *1* (11), 6626−6637.